

Light Scattering Simulation and Measurement of Monodisperse Spheroids using a Phase Doppler Anemometer

Adrian Doicu*, Jan Köser*, Thomas Wriedt**, Klaus Bauckhage*

Dedicated to Professor Fritz Ebert on the occasion of his 60th birthday

(Received: 11 February 1998; resubmitted: 30 September 1998)

Abstract

Mathematical tools are provided for the computation of the scattered field produced by non-spherical particles moving through the measurement volume of a phase Doppler anemometer. The phase distribution of a spheroid with random orientation is computed by using the rigorous extended boundary condition

method and the ray theory. In a phase Doppler experiment the spheroid parameters are obtained by fitting the measured phase distribution with the simulated phase distribution. The numerical simulations are supported by experimental results on monodisperse spheroids.

1 Introduction

A subject of considerable interest is the measurement of non-spherical particles, since in many practical multiphase flows particles have irregular and complex structures. Several studies [1, 2] have demonstrated that the response of a phase Doppler anemometer (PDA) is very sensitive to the particle shape. This technique is attractive because measurements of phase are more reliable than other scattering characteristics, such as scattered power and signal visibility. Phase shift measurements are relatively insensitive to electronic noise and variations in the intensity of illumination. In this context, the phase Doppler technique appears applicable to non-spherical particles.

Naqwi [3] applied a stochastic approach to phase Doppler measurements for in situ sizing of irregular particles. A strong irregular particle is characterized by the diameter of the equivalent sphere. The size distribution of a collection of particles is obtained from the measured phase distribution by solving a Fredholm integral equation of the first kind. The kernel of the integral equation, representing the broadening of the phase for a given particle size due to its structure, is modeled from the experimental data. However, it is desirable to estimate this monosize phase distribution function using a model light scattering process.

In this paper, the response of a phase Doppler system to spheroidal particles with different orientations is examined. According to *Naqwi* [3], a spheroidal particle can be regarded as a regular non-spherical particle. The aim of this work was to investigate the applicability of light scattering models for computing the phase distribution of spheroidal particles. The organization of the paper is as follows. In Section 2 we formulate the problem of regular non-spherical particle measurement. In Section 3 we use the rigorous extended boundary condition method and the approximate ray

theory to model the phase Doppler signal. Specifically, the phase probability density function for a spheroid with a uniform distribution of the orientation angles is computed. The application of these theoretical models to the measurement of monodisperse spheroids is discussed in Section 4.

2 Measurement of Regular Non-Spherical Particles

We define the class of regular non-spherical particles as a set of particles with parametrized surfaces. In view of the phase Doppler technique, we choose as a standard parameter the diameter of the equivolumetric sphere D and denote the other parameters ε_i , $i = 1, 2, \dots$ as the particle non-sphericity parameters. Let us assume that there is a single non-sphericity parameter ε , and since our analysis is focused on the measurement of spheroidal particles, ε designates the particle eccentricity or the axial ratio of the spheroid.

Let us consider a phase Doppler experiment on a collection of spheroids with random orientations. We assume that the phase difference Φ , the equivolumetric sphere diameter D and the eccentricity ε are random continuous variables, and organize the random vector $[\Phi, D, \varepsilon]$. Furthermore, we assume the existence of a joint density $q(\Phi, D, \varepsilon) \geq 0$, such that the marginal densities are determined as follows:

$$\begin{aligned} p(\Phi) &= \iint q(\Phi, D, \varepsilon) dD d\varepsilon, \\ p(D) &= \iint q(\Phi, D, \varepsilon) d\Phi d\varepsilon, \\ p(\varepsilon) &= \iint q(\Phi, D, \varepsilon) d\Phi dD. \end{aligned} \quad (1)$$

The conditional density of Φ , given that $D = D_0$ and $\varepsilon = \varepsilon_0$, is denoted by

$$Q(\Phi, D_0, \varepsilon_0) = q(\Phi, D_0, \varepsilon_0) / \int q(\Phi, D_0, \varepsilon_0) d\Phi. \quad (2)$$

* Dr.-Ing. A. Doicu, Dipl.-Phys. J. Köser, Prof. Dr.-Ing. K. Bauckhage, Universität Bremen, Verfahrenstechnik, Badgasteiner Str. 3, D-28359 Bremen (Germany).

** Dr.-Ing. T. Wriedt, Institut für Werkstofftechnik, Badgasteiner Str. 3, D-28359 Bremen (Germany).

Let us introduce the joint density $\hat{q}(\Phi, D)$ of the random vector $[\Phi, D]$ by

$$\hat{q}(\Phi, D) = \int q(\Phi, D, \varepsilon) d\varepsilon \quad (3)$$

and the conditional density of Φ , given that $D = D_0$, $\hat{Q}(\Phi, D_0)$, by

$$\hat{Q}(\Phi, D_0) = \hat{q}(\Phi, D_0)/p(D_0). \quad (4)$$

Similarly, we denote by $\hat{q}(\Phi, \varepsilon)$,

$$\hat{q}(\Phi, \varepsilon) = \int q(\Phi, D, \varepsilon) dD, \quad (5)$$

the joint density of the random vector $[\Phi, \varepsilon]$, and by $\hat{Q}(\Phi, \varepsilon_0)$,

$$\hat{Q}(\Phi, \varepsilon_0) = \hat{q}(\Phi, \varepsilon_0)/p(\varepsilon_0), \quad (6)$$

the conditional density of Φ given that $\varepsilon = \varepsilon_0$.

The phase density function $p(\Phi)$ is obtained by the measurement of the phase shift between the Doppler signals. The conditional density $Q(\Phi, D_0, \varepsilon_0)$ can be computed numerically by using a rigorous or an approximate method of light scattering theory under the assumption that the distribution of the orientation angles is known. Usually, this distribution is assumed to be uniform. Essentially, the conditional density $Q(\Phi, D_0, \varepsilon_0)$ represents the broadening of the phase Φ for given D_0 and ε_0 and different orientation angles. Unfortunately, this information is not sufficient for computing both marginal densities $p(D)$ and $p(\varepsilon)$ from Eqs. (1) and (2).

We can simplify the problem by assuming that one of the marginal densities is known. For example, if the marginal density $p(\varepsilon)$ is known, it is possible to compute the conditional density $\hat{Q}(\Phi, D_0)$ using a model of light scattering theory. By combining Eqs. (1), (3) and (4) we obtain the density $p(D)$ as a solution to the Fredholm integral equation:

$$p(\Phi) = \int \hat{Q}(\Phi, D_0)p(D_0) dD_0. \quad (7)$$

Similarly, assuming that the marginal density $p(D)$ is known, we compute the conditional density $\hat{Q}(\Phi, \varepsilon_0)$ and use Eqs. (1), (5) and (6) to obtain a Fredholm integral equation for the density $p(\varepsilon)$:

$$p(\Phi) = \int \hat{Q}(\Phi, \varepsilon_0)p(\varepsilon_0) d\varepsilon_0. \quad (8)$$

Computations of the marginal densities in the frame of light scattering theories play an important role. The explanation lies in the fact that a correct evaluation of the kernels appearing in the integral equations (7) and (8) is decisive for solving the corresponding inversion problems. In order to confirm the validity of the theoretical models, it is necessary to compare the computed and the measured conditional densities. The analysis can be focused on the conditional density $Q(\Phi, D_0, \varepsilon_0)$, since, for example, $\hat{Q}(\Phi, D_0)$ may be computed from $Q(\Phi, D_0, \varepsilon_0)$ by varying the parameter ε according to a prescribed probability density function. The validity of conditional density evaluation will be discussed in Section 4.

3 Scattering Theories

Many techniques have been developed for analyzing scattering by dielectric particles. At present the extended boundary condition method (EBCM) is one of the most efficient and powerful tools for rigorously computing non-spherical scattering based on directly solving Maxwell's equations [4, 5]. The main advantages of the

EBCM are high and easily controllable numerical accuracy, superior numerical efficiency and analyticity of the mathematical formulation. However, for large size parameters, the approximate methods for calculating the far-zone scattered intensity have superior computational efficiency to the rigorous methods. One of these approximate methods is the ray theory [6, 7]. In this section, we present fundamentals of these approaches in the context of their applicability to phase Doppler anemometry.

3.1 Extended Boundary Condition Method

To describe the scattering of light by an arbitrary nonspherical particle, we choose a coordinate system having its origin inside the particle. Consider a plane electromagnetic wave incident in the direction specified by a unit vector \mathbf{n}_i ,

$$\mathbf{E}_i(\mathbf{r}) = (E_\theta^i \mathbf{i}_\theta + E_\varphi^i \mathbf{i}_\varphi) e^{i k_0 \mathbf{n}_i \cdot \mathbf{r}} \quad (9)$$

where $\mathbf{n}_i = \mathbf{n}_i(\theta_i, \varphi_i)$, k_0 is the free-space wavenumber for free-space wavelength λ_0 , \mathbf{r} is the radius vector with its origin at the origin of the coordinate system and \mathbf{i}_θ and \mathbf{i}_φ are the unit vectors in the θ and φ directions.

In the framework of the T-matrix approach, the scattering object is replaced by a set of electric and magnetic surface current densities \mathbf{e} and \mathbf{h} over the particle surface, so that in the exterior region the sources and fields are the same as those existing in the original scattering problem. Let us introduce notations relating the total electric field to the surface current densities:

$$\mathbf{E}(\mathbf{r}) = \mathbf{E}_i(\mathbf{r}) + \nabla \times \int_S \mathbf{e}(\mathbf{r}') g(\mathbf{r}', \mathbf{r}) dS' - \nabla \times \nabla \times \int_S \frac{1}{jk_0 \varepsilon_0} \mathbf{h}(\mathbf{r}') g(\mathbf{r}', \mathbf{r}) dS' \quad (10)$$

where $g(\mathbf{r}', \mathbf{r})$ is the free space Green's function, ε_0 is the permittivity of the surrounding medium and S is the surface of the scatterer. For \mathbf{r} outside S , $\mathbf{E}(\mathbf{r})$ represents the total electric field, whereas for \mathbf{r} inside S , the null-field condition is $\mathbf{E}(\mathbf{r}) = 0$.

An approximate solution of the scattering problem can be obtained by considering the null-field condition for the total electric field inside a spherical surface inscribed in S . Expanding the incident field in terms of regular spherical vector wavefunctions $\mathbf{M}_{mn}^1(k_0 \mathbf{r})$ and $\mathbf{N}_{mn}^1(k_0 \mathbf{r})$, i.e.

$$\mathbf{E}_i(\mathbf{r}) = \sum_{m \in \mathbb{Z}} \sum_{n \geq \max(1, |m|)} D_{mn} [a_{mn} \mathbf{M}_{mn}^1(k_0 \mathbf{r}) + b_{mn} \mathbf{N}_{mn}^1(k_0 \mathbf{r})], \quad (11)$$

and using the spherical wave expansions of Green's function, we obtain a set of integral equations for the surface current densities \mathbf{e} and \mathbf{h} . The infinite system of integral equations is truncated and solved by approximating the surface current densities by the complete set of tangential single spherical coordinate vector wavefunctions of the interior problem.

Once the surface current densities have been determined, the scattered field can be computed by using the integral representation (10) for \mathbf{r} lying outside a spherical surface enclosing S . Essentially, the expansion coefficients of the scattered field in terms of radiating spherical vector wavefunctions $\mathbf{M}_{mn}^3(k_0 \mathbf{r})$ and $\mathbf{N}_{mn}^3(k_0 \mathbf{r})$,

$$\mathbf{E}_s(\mathbf{r}) = \sum_{m' \in \mathbb{Z}} \sum_{n' \geq \max(1, |m'|)} D_{m'n'} [f_{m'n'} \mathbf{M}_{m'n'}^3(k_0 \mathbf{r}) + g_{m'n'} \mathbf{N}_{m'n'}^3(k_0 \mathbf{r})], \quad (12)$$

are related to the incident field coefficients by a transition matrix $[\mathbf{T}]$ as follows:

$$\begin{bmatrix} f_{m'n'} \\ g_{m'n'} \end{bmatrix} = \begin{bmatrix} \mathbf{T}_{m'n'}^{mn} \end{bmatrix} \begin{bmatrix} a_{mn} \\ b_{mn} \end{bmatrix}. \quad (13)$$

In the far-field region, the scattered wave becomes spherical and is given by

$$\mathbf{E}_s(\mathbf{r}) = [E_\theta^s \mathbf{i}_\theta + E_\varphi^s \mathbf{i}_\varphi] \frac{e^{jk_0 r}}{k_0 r} \quad (14)$$

$$\begin{bmatrix} E_\theta^s \\ E_\varphi^s \end{bmatrix} = [\mathbf{S}(\mathbf{n}_s, \mathbf{n}_i)] \begin{bmatrix} E_\theta^i \\ E_\varphi^i \end{bmatrix} \quad (15)$$

where $\mathbf{n}_s = \mathbf{r}/r = \mathbf{n}_s(\theta_s, \varphi_s)$ is the scattering direction and $[\mathbf{S}(\mathbf{n}_s, \mathbf{n}_i)]$ is a (2×2) amplitude scattering matrix which linearly transforms the electric vector components of the incident wave into the electric vector components of the scattered wave. A fundamental feature of the T -matrix approach is that the elements of the T matrix are independent of the incident and scattered fields and depend only on the shape, size parameter and refractive index of the scattering particle and on its orientations with respect to the coordinate system. Consequently, the T matrix need be computed only once and then can be used in computations for any particle orientation. The above analysis can be simply extended to a dual-wave system in order to model the signal of PDA [7].

3.2 Ray Theory

For large size parameters, the ray theory accounting for diffraction, reflection and transmission gives a good approximation of the far zone intensity in the forward scattering hemisphere. The expressions of transmitted, reflected and diffracted electric fields can be generally written as

$$\mathbf{E}_s(\mathbf{r}) = jE_0 \frac{e^{jk_0 r}}{k_0 r} S(\theta_s, \varphi_s) e^{j\delta(\theta_s, \varphi_s)} \mathbf{e}_p(\theta_s, \varphi_s) \quad (16)$$

where $S(\theta_s, \varphi_s)$, $\delta(\theta_s, \varphi_s)$ and $\mathbf{e}_p(\theta_s, \varphi_s)$ are the amplitude, the phase and the polarization vector of electric-field contributions, respectively. The algorithm for deriving the far-zone electric field for diffraction, reflection and transmission was given in a previous paper [7]. We note here only the expression of the phase of the transmitted ray, which is given by

$$\delta_{tr}(\theta_s, \varphi_s) = \delta_{tr}(\mathbf{n}_i, \mathbf{n}_s) = k_0 L_{trans} - (n + 1) \frac{\pi}{2} \quad (17)$$

where n is an integer indicating the number of caustic participations,

$$L_{trans} = \mathbf{r}_A \mathbf{n}_i - \mathbf{r}_B \mathbf{n}_s + mL_{AB} \quad (18)$$

m is the refractive index, and L_{AB} is the distance of travel of the ray inside the particle. Here, \mathbf{r}_A is the position vector of the point A lying on the particle surface where the incident ray strikes the particle and \mathbf{r}_B is the position vector of the point B where the transmitted ray exits the particle. For a spheroidal particle with spheroid eccentricity satisfying $\varepsilon^2 < m/(m-1)$, $n = 2$, therefore the transmitted phase shift for an arbitrary spheroid orientation is $-3\pi/2$.

A simplified model for analyzing the response of a phase Doppler anemometer can be constructed by assuming that the refraction

mechanism is dominant. In the case of dominant refraction the electric-field contributions due to diffraction and reflection can be neglected and, consequently, the phase of the scattered field is given by Eq. (17). Let us consider a typical PDA configuration in which a particle is illuminated by two incident waves traveling in the \mathbf{n}_i^1 and \mathbf{n}_i^2 directions and the scattered field is analyzed in the \mathbf{n}_s^A and \mathbf{n}_s^B directions. The phase difference between the signals of two points detectors can be expressed as

$$\begin{aligned} \Phi = \Phi_A - \Phi_B = & [\delta_{tr}(\mathbf{n}_i^1, \mathbf{n}_s^A) - \delta_{tr}(\mathbf{n}_i^2, \mathbf{n}_s^A)] \\ & - [\delta_{tr}(\mathbf{n}_i^1, \mathbf{n}_s^B) - \delta_{tr}(\mathbf{n}_i^2, \mathbf{n}_s^B)]. \end{aligned} \quad (19)$$

By convention, the above model will be called the pure refraction model.

3.3 Theoretical Simulation

In this section, we compare the response of a phase Doppler system computed by using the rigorous extended boundary condition method and the pure refraction model. The comparison will be performed by analyzing the phase signal for different orientations of the symmetry axis of the particle. Specifically, the probability density function of the random variable phase difference is computed for different values of the orientation angles α and β . We note here that, since we are interested in the histogram reconstruction and not in the evaluation of a few statistical moments of the random variable phase difference, the analytical method of averaging the scattering matrices given by *Mishchenko* [8] cannot be used. Therefore, we expect that the extended boundary condition method will be very time consuming, especially for spheroids with large size parameters.

An optical configuration with a half-beam crossing angle of 3° , an off-axis angle of 40° and an elevation angle of 10° is considered. This optical arrangement is in accordance with the experimental set-up described in Section 4. The receiving-cone angle is taken as 5.7° . We compute the phase difference for spheroidal particles with (a) $a = 2.2 \mu\text{m}$, (b) $a = 2.4 \mu\text{m}$ and (c) $a = 2.6 \mu\text{m}$, where a is the semi-major axis of the spheroid. The particle eccentricities are (a) $\varepsilon = 1.8$, (b) $\varepsilon = 2.0$ and (c) $\varepsilon = 2.2$, respectively. In our numerical simulations, we consider polystyrene particles ($m_{\text{polystyrene}} = 1.56$) dispersed in water ($m_{\text{water}} = 1.33$). Hence the refractive index is taken as $m = m_{\text{polystyrene}}/m_{\text{water}} = 1.173$. The wavelength of the incident radiation is chosen to be $\lambda = 367 \text{ nm}$, corresponding to the relative wavelength of an argon ion laser ($\lambda = 488 \text{ nm}$) in water. Note that in all cases the equivolumetric spheres have a diameter of about $3 \mu\text{m}$. This gives a phase difference of 79° . The histograms are computed for $N_\alpha = 10$ values of the orientation angle α in the interval $[0, 2\pi]$ and $N_\beta = 20$ values of the orientation angle β in the interval $[0, \pi]$. The computational time of the extended boundary condition method is about 24–25 h, while the computational time of the pure refraction model is a few minutes. The data plotted in Figure 1 show that there is reasonable agreement between the phase distributions computed by using the approximate pure refraction model and the rigorous extended boundary condition method. The peaks of the distributions agree well, and the relative errors of the mean and standard deviation are less than 2.5% and 10%, respectively.

From the above numerical analysis, one may conclude that the pure refraction model can be used to compute the response of a phase Doppler system for particles with spheroid-size parameter ka larger than 40. The higher computational speed makes it economically viable for PDA calculations.

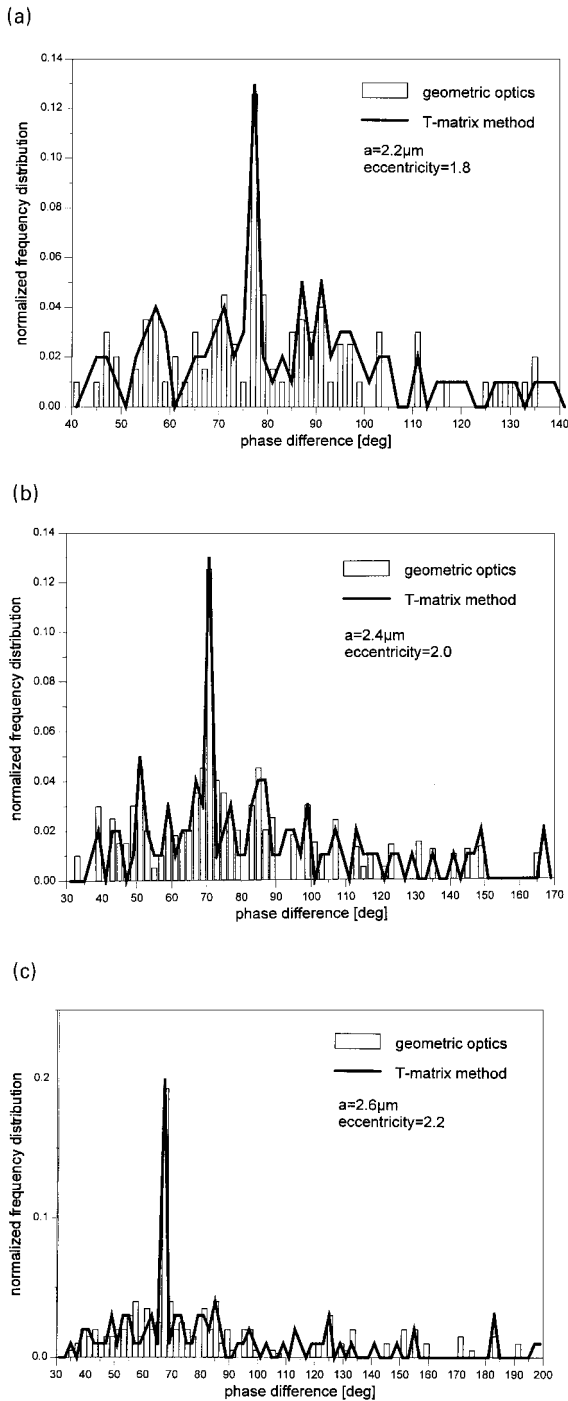


Fig. 1: Frequency distributions of the phase difference for spheroidal particles with: (a) $a = 2.2 \mu\text{m}$, $\varepsilon = 1.8$, (b) $a = 2.4 \mu\text{m}$, $\varepsilon = 2.0$ and (c) $a = 2.6 \mu\text{m}$, $\varepsilon = 2.2$. The histograms are computed with the extended boundary condition method and the pure refraction model for $N_\alpha = 10$ values of the orientation angle α in the interval $[0, 2\pi]$ and $N_\beta = 20$ values of the orientation angle β in the interval $[0, \pi]$.

4 PDA Measurements

In this section, we investigate the validity of the phase distribution evaluation. Our analysis is organized as follows. Consider a phase Doppler experiment on a single particle which rotates during the measuring process. In this context, the use of an electrodynamic levitator in a PDA configuration seems to be a promising method, since the particle rotates inside the trap during the oscillation in the vertical direction [1]. Clearly, the measurement of the phase shift

between the Doppler signals gives the conditional density $Q_m(\Phi, D_0, \varepsilon_0)$. Assume that the spheroid parameters D_0 and ε_0 are known and compute the theoretical conditional density $Q(\Phi, D_0, \varepsilon_0)$. Determine the measured spheroid parameters as a result of a minimization process:

$$D_0, \varepsilon_0 : \min \int |Q(\Phi, D_0, \varepsilon_0) - Q_m(\Phi, D_0, \varepsilon_0)|^2 d\Phi. \quad (20)$$

Then, the deviations between the measured and the theoretical parameters indicate the accuracy of the theoretical models. However, we can assume that the phase difference histogram of a single rotating particle can be reproduced by measurements on monodisperse spheroidal particles. Therefore, we will perform measurements on suspensions of monodisperse spheroids in order to reconstruct the conditional density $Q(\Phi, D_0, \varepsilon_0)$. On the other hand, the above method can be regarded as an efficient tool for measuring the spheroid parameters D and ε .

Our experimental set-up consists of a standard PDA system. We used an air-cooled argon ion laser (100 mW at $\lambda = 488 \text{ nm}$) and a radial diffraction grating to split the incident laser beam. The main frequency of the Doppler signal can be shifted by means of rotation of the radial diffraction grating in order to separate opposite velocity components. However, this is of no importance for the application presented here. The diffracted beams are projected on to the location of the so-called measurement volume by means of a single achromatic lens ($f = 160 \text{ mm}$, $\phi = 80 \text{ mm}$). Hence the beam crossing angle can be selected via the separation between the radial diffraction grating and the lens according to the law of imagery. The maximum value is 26° . For the measurements presented below we chose a half-beam crossing angle of 4° . The polarization of the beams is perpendicular with respect to the mean scattering plane. Two individually mounted photomultiplier tubes are used for detection of the scattered light. Their front lenses are of 60 mm aperture and have a focal length of 300 mm. The photomultipliers are located at an off-axis angle of 60° under $\pm 13.5^\circ$ elevation. The signals are band-filtered and amplified before digitization by means of a 30 MHz AD-board with a 12-bit dynamic range. Data evaluation is performed by means of a standard FFT algorithm.

We performed measurements on monodisperse spheroidal polystyrene particles. The method for preparation of the spheroidal particles with a narrow size distribution for both axes has been described [9]. Monodisperse polystyrene particles with a mean diameter of $D = 3.5 \mu\text{m}$ were dispersed in a solution of polyvinyl alcohol. This dispersion was then allowed to form, by evaporation, a thin film of polyvinyl alcohol containing spherical polystyrene particles. Strips of this film were clamped into a metal frame, heated rapidly in an oil bath to $200 \pm 3^\circ\text{C}$ and stretched to a predetermined extent in order to convert the spherical particles into spheroids with semi-axes $a = (D/2)(\varepsilon)^{2/3}$, $b = (D/2)/(\varepsilon)^{1/3}$. The stretched film strips were washed in iso-propanol to remove any oil left on the surface and then heated to about 85°C until all the film strips had dissolved. The dispersion of polystyrene latex particles was decanted and the sediment latex particles were redispersed in a fresh iso-propanol-water mixture and centrifuged. The sediment was redispersed in distilled water and then centrifuged to sediment the particles. The particles were characterized by electron microscopy. Figure 2 shows an electron micrograph of the particles after stretching.

For our PDA measurements, we used monodisperse spheroids with the following size ranges for the eccentricities: (a) $\varepsilon \pm 3\sigma_\varepsilon = 1.76 \pm 0.2$, (b) $\varepsilon \pm 3\sigma_\varepsilon = 1.94 \pm 0.25$ and (c) $\varepsilon \pm 3\sigma_\varepsilon = 2.3 \pm 0.3$. The monodisperse spheroids were dispersed in distilled water.

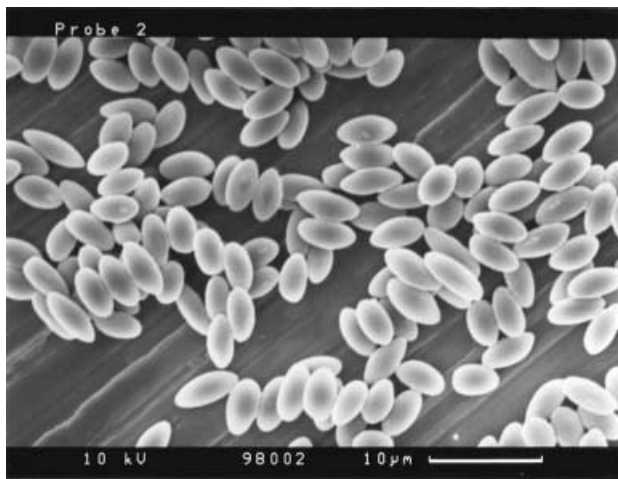


Fig. 2: Electron micrograph of the monodisperse spheroids.

A cylindrical quartz flow cuvette (8 mm clear diameter, 74 mm length) was mounted on a squeezed tube pump. The flow was directed upwards, in a direction perpendicular to the system of interference fringes. The typical signal frequency was about 30 kHz. All angular set-up data has to be corrected for refraction at the air-glass-water interface. Note that the phase difference for the equivolumetric sphere ($D = 3.5 \mu\text{m}$) is 92° . Typical PDA results for monodisperse spheroids are presented in Figure 3.

The dashed lines represent numerically simulated phase difference distributions, which approximate in the mean square sense the measured phase distributions. We chose the equivalent diameter in the range $D = 3.1, 3.3, \dots, 3.9 \mu\text{m}$ and the eccentricity in the range $\varepsilon = 1.4, 1.6, \dots, 2.6$. We found the optimal values to be $D = 3.5 \mu\text{m}$ and $\varepsilon = 1.8, 2.0$ and 2.2 , respectively. From the above analysis, one may conclude that there is reasonable agreement between the measured data and the simulation.

5 Conclusions

Mathematical tools have been used for computing the scattered field produced by a spheroid moving through the measurement volume of a phase Doppler anemometer. Specifically, the phase probability density function was computed for different orientations of the symmetry axis using the rigorous extended boundary condition method and the approximate ray theory. It has been shown that for particles with spheroid size parameters larger than 40 the results obtained with the geometrical optics model agree, within certain bounds, with those obtained by using the rigorous model.

The validity of the theoretical models was investigated by measurements on monodisperse spheroids. The spheroids parameter were obtained by fitting the measured phase probability density function with a theoretical density. The agreement with the values obtained by electron microscopy confirms the accuracy of the light scattering models.

The developed mathematical tools can be used for measuring the size distribution of equivolumetric spheres. As the EBCM can handle particles with various geometries, the above formalism can be extended with minor corrections to other types of regular non-spherical particles. In this case we have to compute the phase density function for different orientations and statistics of the non-sphericity parameters. It will be interesting to see if for non-spherical particles with the same equivolumetric sphere

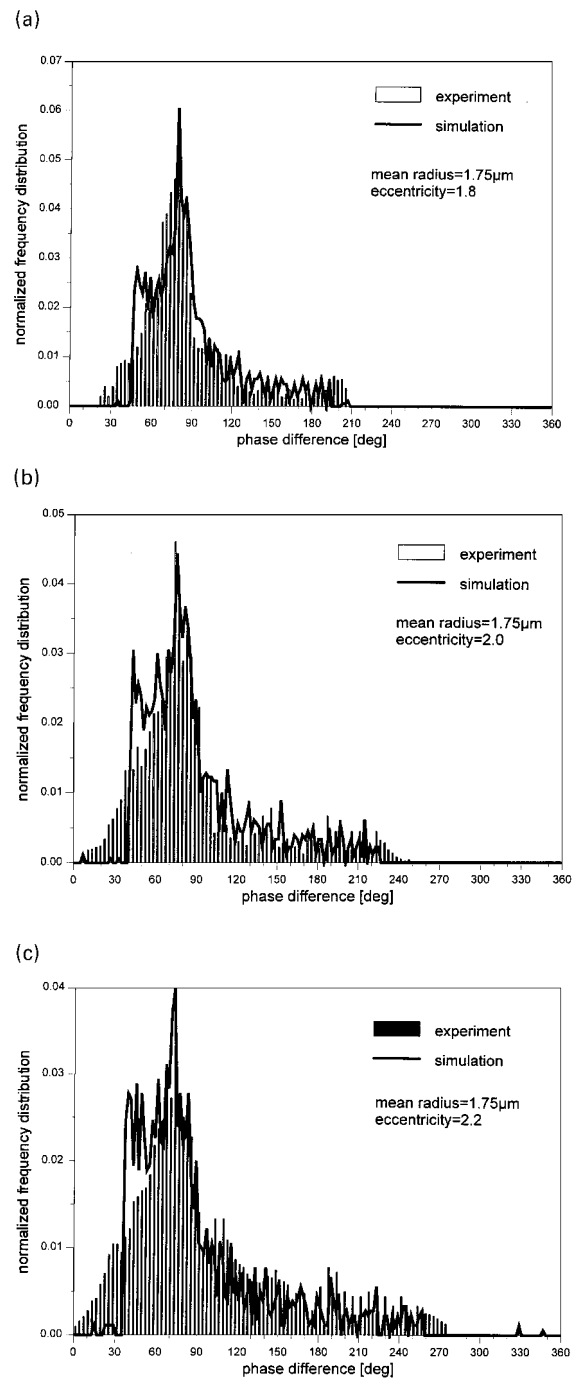


Fig. 3: Frequency distributions of the phase difference for monodisperse spheroids with the equivalent diameter $D = 3.5 \mu\text{m}$ and the following size ranges for the eccentricities: (a) $\varepsilon \pm 3\sigma_\varepsilon = 1.76 \pm 0.2$, (b) $\varepsilon \pm 3\sigma_\varepsilon = 1.94 \pm 0.25$ and (c) $\varepsilon \pm 3\sigma_\varepsilon = 2.3 \pm 0.3$. The dashed lines represent numerically simulated phase difference distributions which approximate in the mean square sense the measured phase distributions. The optimal values for the particle eccentricities are found to be $\varepsilon = 1.8, 2.0$ and 2.2 , respectively.

diameter but different shapes the phase distributions differ significantly.

6 Acknowledgments

The authors are grateful to the Deutsche Forschungsgemeinschaft for providing financial support for this work.

7 Symbols and Abbreviations

a, b	semi-major axis and semi-minor axis of the spheroid	\mathbf{r}_A	position vector of the point A where the incident ray strikes the particle surface
(a_{mn}, b_{mn})	expansion coefficients of the incident field	\mathbf{r}_B	position vector of the point B where the transmitted ray exits the particle surface
D, D_0	diameters of the equivolometric sphere	α, β	orientation angles of the spheroid symmetry axis
D_{mn}	normalization constant	$\delta(\theta_s, \varphi_s)$	phase of the electric field contribution
\mathbf{E}	total electric field	$\delta_{ir}(\theta_s, \varphi_s)$	phase of the transmitted ray
$\mathbf{E}_i, \mathbf{E}_s$	incident and scattered fields	ε_i	non-sphericity parameter
$(E_\theta^i, E_\varphi^i)$	components of the incident field in θ and φ directions	$\varepsilon, \varepsilon_0$	particle eccentricity
$(E_\theta^s, E_\varphi^s)$	components of the scattered field in θ and φ directions	ε_0	permittivity of the surrounding medium
(\mathbf{e}, \mathbf{h})	surface current densities	λ_0	wavelength in vacuum
$\mathbf{e}_p(\theta_s, \varphi_s)$	polarization vector of the electric field contribution	(θ_i, φ_i)	angular coordinates of the incident vector \mathbf{n}_i
(f_{mn}, g_{mn})	expansion coefficients of the scattered field	(θ_s, φ_s)	angular coordinates of the scattered vector \mathbf{n}_s
$g(\mathbf{r}', \mathbf{r})$	Green's function	σ_ε	standard deviation of the particle eccentricity
$(\mathbf{i}_\theta, \mathbf{i}_\varphi)$	unit vectors in θ and φ directions	Φ	phase difference
k_0	free-space wavenumber		
L_{trans}, L_{AB}	optical lengths		
$(\mathbf{M}_{1mn}^1, \mathbf{N}_{1mn}^1)$	regular and radiating spherical vector		
$(\mathbf{M}_{3mn}^3, \mathbf{N}_{3mn}^3)$	wavefunctions, respectively		
m	refractive index		
n	number of caustic participations		
$\mathbf{n}_i, \mathbf{n}_s$	unit vectors of the incident and the scattering directions, respectively		
$p(\Phi), p(D), p(\varepsilon)$	marginal densities of the random vector $[\Phi, D, \varepsilon]$		
$Q(\Phi, D_0, \varepsilon_0)$	conditional density of the random vector $[\Phi, D, \varepsilon]$ given that $D = D_0$ and $\varepsilon = \varepsilon_0$		
$\hat{Q}(\Phi, D_0)$	conditional density of the random vector $[\Phi, D]$ given that $D = D_0$		
$\hat{Q}(\Phi, \varepsilon_0)$	conditional density of the random vector $[\Phi, \varepsilon]$ given that $\varepsilon = \varepsilon_0$		
$q(\Phi, D_0, \varepsilon_0)$	joint density of the random vector $[\Phi, D, \varepsilon]$		
$\hat{q}(\Phi, D_0)$	joint density of the random vector $[\Phi, D]$		
$\hat{q}(\Phi, \varepsilon_0)$	joint density of the random vector $[\Phi, \varepsilon]$		
$[\mathbf{S}(\mathbf{n}_i, \mathbf{n}_s)]$	amplitude scattering matrix		
S	particle surface		
$S(\theta_s, \varphi_s)$	amplitude of the electric field contribution		
$[\mathbf{T}]$	transition matrix		
\mathbf{r}	position vector		

8 References

- [1] G. Göbel, A. Doicu, T. Wriedt, K. Bauckhage: Influence of surface roughness of conducting spheres on the response spheres of a phase Doppler anemometer. Part. Part. Syst. Charact. 14 (1997) 283–289.
- [2] S. R. Martin, L. E. Drain, M. L. Yeoman, D. M. Livesley: Resolution limits of the phase Doppler technique and its extension to monitor non-ideal particles in two phase flows. Proc. 4th Int. Symp. on Application of Laser Anemometry to Fluid Mechanics. Lisbon (1988) paper 2.8.
- [3] A. A. Naqwi: Sizing of irregular particles using a phase Doppler system. Part. Part. Syst. Charact. 13 (1996) 343–349.
- [4] P. C. Waterman: Symmetry, unitary and geometry in electromagnetic scattering. Phys. Rev. D 3 (1970) 825–839.
- [5] P. Barber, C. Yeh: Scattering of electromagnetic waves by arbitrarily shaped dielectric bodies. Appl. Opt. 14 (1975) 2864–2872.
- [6] J. A. Lock: Ray scattering by an arbitrarily oriented spheroid. II. Transmission and cross-polarization effects. Appl. Opt. 35 (1996) 515–531.
- [7] A. Doicu, T. Wriedt, K. Bauckhage: Light scattering by homogeneous axisymmetric particles for PDA calculations to measure both axes of spheroidal particles. Part. Part. Syst. Charact. 14 (1997) 3–11.
- [8] M. I. Mishchenko: Light scattering by randomly oriented axially symmetric particles. J. Opt. Soc. Am. A 8 (1991) 871–882.
- [9] C. C. Ho, A. Keller, J. A. Odell, R. H. Ottewill: Preparation of monodisperse ellipsoidal polystyrene particles. Colloid Polym. Sci. 271 (1993) 469–479.